Journal of Materials Chemistry C

COMMUNICATION

View Article Online
View Journal | View Issue

Cite this: J. Mater. Chem. C, 2019, 7, 3160

Received 16th January 2019,
Accepted 4th February 2019

DOI: 10.1039/c9tc00291j

rsc.li/materials-c

Tunable negative permittivity and magnetic performance of yttrium iron garnet/polypyrrole metacomposites at the RF frequency

Chuanbing Cheng,[ab] Runhua Fan,*[c] Guohua Fan,[b] Hu Liu,[de] Jiaoxia Zhang,[ef] Jianxing Shen,[a] Qian Ma,[g] Renbo Wei*[h] and Zhanhu Guo*[e]

Polypyrrole (PPy) composites incorporating yttrium iron garnet (YIG) particles were prepared by an *in situ* oxidative polymerization method. The effects of YIG particle loading level on the radio-frequency (RF) electromagnetic properties of the YIG/PPy composites were systematically investigated. A negative permittivity behaviour combined with metal-like conduction was observed in the PPy composites, which was due to the low-frequency plasmonic state of free electrons in the formed conducting PPy networks. The Drude model was used to give a good description of the dielectric response. After increasing the YIG loading, the plasma frequency, at which the real part of permittivity changed from negative to positive, shifted to a lower frequency, and the magnitude (absolute value) of negative permittivity also became smaller. In addition, the permeability of the composites showed a relaxation-type frequency dispersion, which was attributed to the combined effect of the magnetic resonance of YIG particles and diamagnetic response of PPy conducting networks. This work can pave the way for exploiting the regulation mechanism of negative permittivity, benefiting the practical applications of polymer metamaterials.

1. Introduction

Metamaterials with negative electromagnetic parameters (*i.e.*, permittivity and permeability) have experienced a huge growth in research activity for more than a decade.[1,2] Extraordinary physical properties, such as negative refraction and reversed Doppler effect, have been demonstrated in the metamaterials, paving the way for their applications in the fields of plasmonics, invisibility, optical imaging, microwave absorbers and electromagnetic shielding.[3–10] So far, two types of materials have been developed to obtain negative parameters: ordered metamaterials and random metamaterials or metacomposites.[11–14] For ordered metamaterials, the negative parameters can be achieved by structuring periodically repeating units on a subwavelength scale, which are strongly associated with the geometry of a periodic structure.[15] However, there are some drawbacks that hamper most of their applications. For example, the bandwidth of negative parameters is generally narrow, and the preparation process is complicated and time-consuming.[12] In order to alleviate these limitations, random metamaterials without a periodic structure have been recently proposed and studied. In such metamaterials, the negative parameters can be achieved by classical material design, which focuses on optimizing the chemical composition and the microstructure of materials.[16,17] These works widen the scope of possibilities for constructing metamaterials in a much simpler way.

In the research of random metamaterials, metals and their composites have drawn more attention due to their intrinsic property: metals possess negative permittivity below their plasma frequencies (near visible band).[8,18] A variety of metal and alloy particles were embedded into the insulated polymer or ceramic matrixes, and negative parameters were realized in the obtained metacomposites in various frequency ranges.[19–27] Interestingly, several recent studies have reported negative permittivity in conducting polymers and their composites, which can be considered as ideal candidates for random metamaterials.[28–30] For instance, a plasma-like negative permittivity behavior was found in highly conducting polypyrrole (PPy) and polyaniline (PANI) at a microwave frequency band, which was similar to the behavior of usual metals.[31,32]

[a] Key Laboratory of Processing and Testing Technology of Glass & Functional Ceramics of Shandong Province, School of Materials Science and Engineering, Qilu University of Technology (Shandong Academy of Sciences), Jinan 250353, China
[b] Key Laboratory for Liquid–Solid Structural Evolution and Processing of Materials, (Ministry of Education), Shandong University, Jinan 250061, China
[c] College of Ocean Science and Engineering, Shanghai Maritime University, Shanghai 201306, China. E-mail: rhfan@shmtu.edu.cn
[d] Key Laboratory of Materials Processing and Mold (Zhengzhou University), Ministry of Education, National Engineering Research Center for Advanced Polymer Processing Technology, Zhengzhou University, Zhengzhou 450002, China
[e] Integrated Composites Laboratory (ICL), Department of Chemical & Biomolecular Engineering, University of Tennessee, Knoxville, TN 37996, USA. E-mail: zguo10@utk.edu
[f] College of Material Science and Engineering, Jiangsu University of Science and Technology, Zhenjiang 212003, Jiangsu Province, China
[g] Jinan Sijian Construction Group Co., Ltd, Jinan 250031, China
[h] Research Branch of Advanced Functional Materials, School of Materials and Energy, University of Electronic Science and Technology of China, Chengdu, 611731, P. R. China. E-mail: weirb10@uestc.edu.cn

Guo *et al.*[33–37] realized the negative permittivity behavior in PPy or PANI composites incorporating various inorganic nanoparticles, such as WO_2, Fe_3O_4, $BaTiO_3$ and SiC. Moreover, the negative permittivity behavior has been observed in PPy or PANI composites containing graphene, carbon nanotubes or nanofibers.[38–41] However, in these works, almost no attention was given to adjust the negative permittivity; also, the regulation mechanism of negative permittivity has not been determined to date. Indeed, the tuning of negative permittivity in metamaterials is an important issue for many actual applications.[42] For example, there is a need for tunable and broad frequency band of negative permittivity to ensure multi-frequency operations for a passband filter.[43,44] Moreover, the metamaterials with considerable negative permittivity can be well applied in the field of electromagnetic interference (EMI) shielding,[22,45] while the small negative magnitude of permittivity is beneficial for their application in microwave absorbing.[46] Furthermore, the metacomposites with small absolute values of negative permittivity were recently applied for constructing laminated composites with a high dielectric constant and low loss, and these composites would be suitable for energy-storage capacitors.[47,48]

Yttrium iron garnet ($Y_3Fe_5O_{12}$, YIG) is a versatile ferromagnetic insulator with low magnetic damping and excellent magneto-optic property, and it has been widely used in electronic and microwave devices such as oscillators, filters, antennas, phase shifters and magnetic field sensors.[49–51] Recently, some metamaterials have also been constructed using YIG, and their magnetic property has been well studied.[25,52–55] However, to the best of our knowledge, conductive polymer composites incorporating YIG have not been reported to date.

In this paper, PPy composites were fabricated with different YIG particle loadings using an *in situ* polymerization process. Their microstructure, electrical conductivity, dielectric behavior and magnetic property were comparatively investigated. It was found that PPy conductive networks were formed in the composites, and a negative permittivity behavior combined with metal-like conduction was observed. The frequency range and the value of negative permittivity were well related to the YIG content, which was excellently explicated by the Drude model. Meanwhile, the frequency dispersion of permeability was analyzed by magnetic resonance and diamagnetic response.

2. Experimental

2.1. Materials

Pyrrole monomer (C_4H_5N), ammonium persulfate (APS, $(NH_4)_2S_2O_8$) and *p*-toluene sulfonic acid (PTSA, $C_7H_8O_3S$) were purchased from Sigma-Aldrich Co. LLC. Yttria (Y_2O_3) and iron oxide (Fe_2O_3) powders were obtained from Sinopharm Chemical Reagent Co., Ltd, and their purity was more than 99.0%.

2.2. Specimen preparation

YIG powders were synthesized through a typical solid-state reaction process. First, the mixtures of Y_2O_3 and 62.5 mol% Fe_2O_3 powders were uniformly mixed in ethyl alcohol for 10 h. After drying completely, the obtained powders were sifted with a 100-mesh sieve and then, the mixtures were calcined at 1523 K for 6 h to obtain YIG powders ($3Y_2O_3 + 5Fe_2O_3 \rightarrow 2Y_3Fe_5O_{12}$). Finally, the YIG powders were milled in a mortar and sieved with a 200-mesh sieve.

PPy and its composites were prepared by a surface-initiated polymerization method. First, a certain amount of YIG powders was initially dispersed in 200 mL aqueous solution containing PTSA (30 mmol) and APS (18 mmol), followed by one-hour sonication and mechanical stirring in an ice-water bath. Then, 50 mL pyrrole solution (0.72 mmol mL^{-1}) was poured into the above YIG suspension, and the mixed solution was sonicated and stirred for additional 2 h in an ice-water bath to further polymerize. The color of the solution turned black, which indicated that the polymerization of pyrrole had begun. After that, the resultant solution was filtrated, and the obtained product was washed with deionized water and methyl alcohol to remove any unreacted PTSA, APS and possible oligomers. Finally, the black powders were fully dried at 50 °C for 12 h and were pressed at 100 MPa for 1 min to obtain bulk composites. The PPy composites filled with YIG loadings of 10.86, 43.56, 63.35, 72.03 and 79.93 wt% were synthesized and recorded as PY10, PY43, PY63, PY72 and PY79, respectively. Pure PPy was also prepared using the same process for comparison and was designated as PY0. The samples were processed into wafers (diameter, 25 mm; thickness, 1–2 mm) for electrical measurements and into annular discs (inner diameter, 6 mm; outer diameter, 20 mm; height, 1–2 mm) for permeability measurements.

2.3. Characterization

X-ray diffraction (XRD) analysis was performed on a PANalytical X'Pert MPD Pro X-ray powder diffractometer equipped with an Anton Paar XRK-90 linear detector using a Ni-filtered Cu Ka radiation source. The diffraction patterns were obtained over a 2θ angle range of 10–90° at a sweep speed of 3° min^{-1} at room temperature in the air. The Fourier transform infrared (FTIR) spectra of pure PPy, YIG and their composites in the wavenumber range of 4000–500 cm^{-1} were recorded using a Nicolet iS50 spectrometer coupled with an ATR accessory at a resolution of 5 cm^{-1}. Scanning electron microscopy (SEM) images were obtained using Zeiss Merlin FE-SEM. The direct current (DC) conductivity of the samples was measured by a standard four-probe method using a KEITHLEY 2400 SourceMeter at room temperature. Alternating current (AC) conductivity (σ_{ac}), complex permittivity ($\varepsilon_r^* = \varepsilon_r' - j\varepsilon_r''$) and permeability ($\mu_r^* = \mu_r' - j\mu_r''$) spectra of the specimens were measured using an impedance analyzer (Agilent E4991A) in the frequency band range from 20 MHz to 1 GHz at room temperature. The 16453A test fixture was used for permittivity measurements, and the 16454A test fixture was applied to determine permeability property.

3. Results and discussion

3.1 Composition

Fig. 1 shows the FT-IR spectra of pure PPy, YIG particles and their composites. No clear absorption peak is observed for the YIG particles. Pure PPy and its composites show the same absorption peaks centered at 1528 and 1431 cm^{-1}, which are ascribed to the

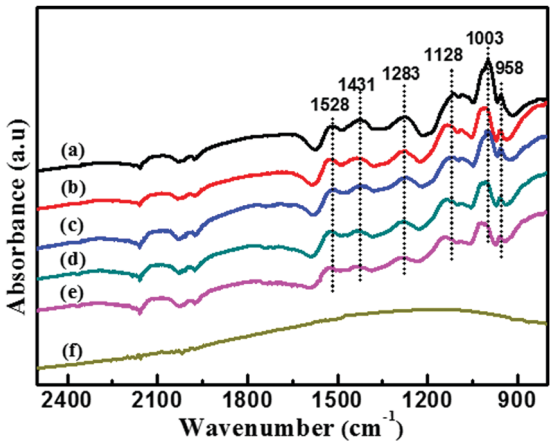

Fig. 1 FT-IR spectra of (a) pure PPy and composites with YIG loadings of (b) 10.86, (c) 43.56, (d) 63.35 and (e) 79.93 wt% and (f) YIG particles.

C=C and C–N stretching vibrations, respectively.[34] The peaks near 1283 and 1003 cm^{-1} can be assigned to the in-plane and out-of-plane C–H vibrations, and the peaks observed at 1128 and 958 cm^{-1} correspond to the breathing vibration of the pyrrole ring and C–C out-of-phase deformation vibration.[56] Meanwhile, it was observed that a shift of FT-IR peaks occurred as a result of the incorporation of YIG particles in the polymer matrix. With the increasing YIG content, the peaks near 1128 and 1009 cm^{-1} shifted to a lower wave number, which was attributed to the interaction between YIG and PPy.[34,56] The XRD patterns of pure PPy, YIG and their composites are presented in Fig. 2. The XRD pattern of pure PPy shows a broad band at 2θ = 20–30°, suggesting a semicrystalline structure of the obtained PPy.[57] For the composites with high YIG particle loadings, strong diffraction peaks of YIG are observed in the XRD pattern, and the characteristic peak of PPy disappears, which can be due to the overlapping of the wide peak of PPy by the high-intensity peaks of YIG.

3.2 Microstructure

The SEM images of pure PPy, YIG and their corresponding composites (PY43 and PY63) are shown in Fig. 3. Pure PPy exhibits particulate structures with a uniform size distribution (no more than 1 μm, Fig. 3a), and YIG particles show an irregular shape of micron size (Fig. 3f). In the composites, the PPy particles or clusters were formed and adhered to the surface of YIG particles. During the chemical polymerization process, PPy particles were more inclined to form on the surface of YIG particles due to the adsorption effect between pyrrole monomers and YIG particles *via* π–π interactions, hydrogen bonds and van der Waals forces.[58] As the YIG loading increased, more YIG particles were exposed to the surrounding, and the size of PPy particles also became smaller.

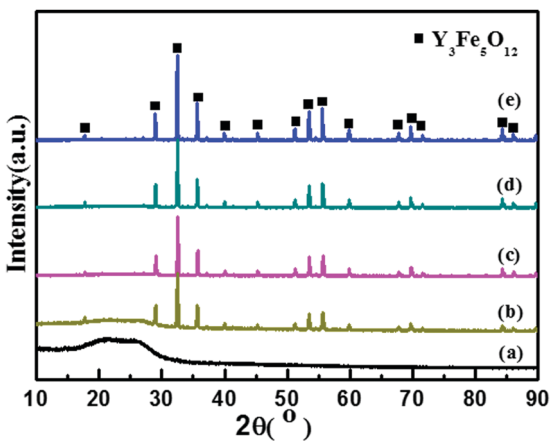

Fig. 2 XRD patterns of (a) pure PPy and composites with particle loadings of (b) 10.86, (c) 43.56 and (d) 63.35 wt% and (e) YIG particles.

3.3 Electrical property

Fig. 4a shows the DC conductivity of composites as a function of the loading of YIG particles. The incorporation of YIG reduced the DC conductivity (σ_{dc}), and the insulated YIG particles deteriorated the interconnection of PPy particles and impeded the movement of free electrons in the composites; thus, σ_{dc} gradually decreased as the YIG content increased.[59] The frequency-dependent AC conductivity (σ_{ac}) for PPy and its composites with various YIG contents is presented in Fig. 4b. The σ_{ac} values of all samples decrease with increasing frequency, showing metal-like conductive behavior.[18] This indicated that three-dimensional conductive PPy networks were formed in the composites.[21,60,61] The decrease in σ_{ac} was due to the skin effect; this is a tendency where the alternating current flows mainly at the near surface region of an electrical conductor. The depth of the surface region is called the skin depth (δ), which is given by[19,62]

$$\delta = \sqrt{\frac{2}{\omega\sigma_{dc}\mu}} \quad (1)$$

where ω ($\omega = 2\pi f$) is the angular frequency, σ_{dc} is the resistivity and μ is the static permeability. The σ_{dc} and μ values were constant for the obtained materials; thus, δ was directly proportional to the square root of f. A higher frequency resulted in lower δ and the enhancement of skin effect, leading to decrease in σ_{ac} for the samples, especially at high frequencies.[63]

Fig. 5 illustrates the frequency-dependent permittivity ($\varepsilon_r^* = \varepsilon_r' - j\varepsilon_r''$) for PPy and its composites with various YIG contents. A plasma-like negative permittivity ε_r' behavior is observed in all samples (Fig. 5a). This is similar to the dielectric response of usual metals. The negative ε_r' value results from the low-frequency plasmonic state provided by the free carriers in the formed PPy networks.[24,26] The ε_r' spectra are fitted using the Drude model:[64]

$$\varepsilon_r' = 1 - \frac{\omega_p^2}{\omega^2 + \omega_\tau^2} \quad (2)$$

Here, ω_p ($\omega_p = 2\pi f_p$) is the effective angular plasma frequency, and ω_τ is the relaxation rate. The fitting curves (solid lines), which are obtained using the OriginPro 9 software by an iterative method according to eqn (2), are in accordance with the experimental result (dotted lines) of ε_r'. The obtained fitting coefficients (R^2) and parameters (ω_p and ω_τ) are shown in Table 1. The fitting ω_p and ω_τ values become smaller as YIG loading increases. Also, ω_p is the collective oscillation

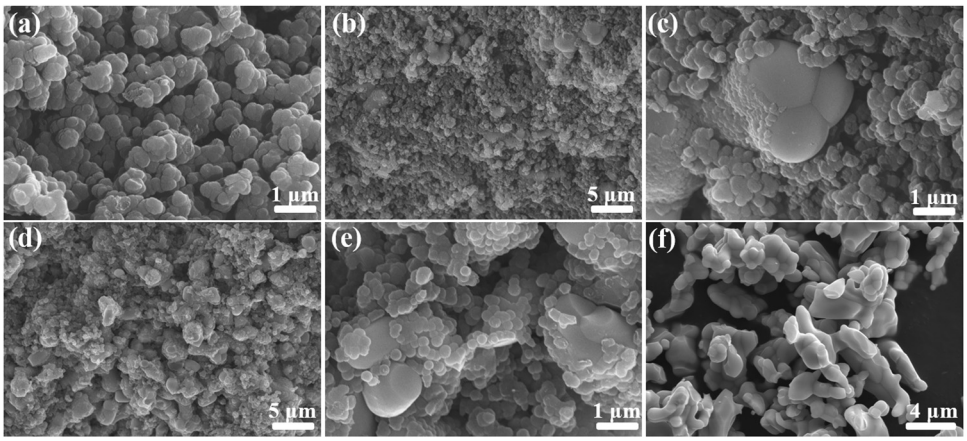

Fig. 3 SEM micrographs of (a) pure PPy and YIG/PPy composites with loadings of (b and c) 43.56, (d and e) 63.35 wt% and (f) YIG particles.

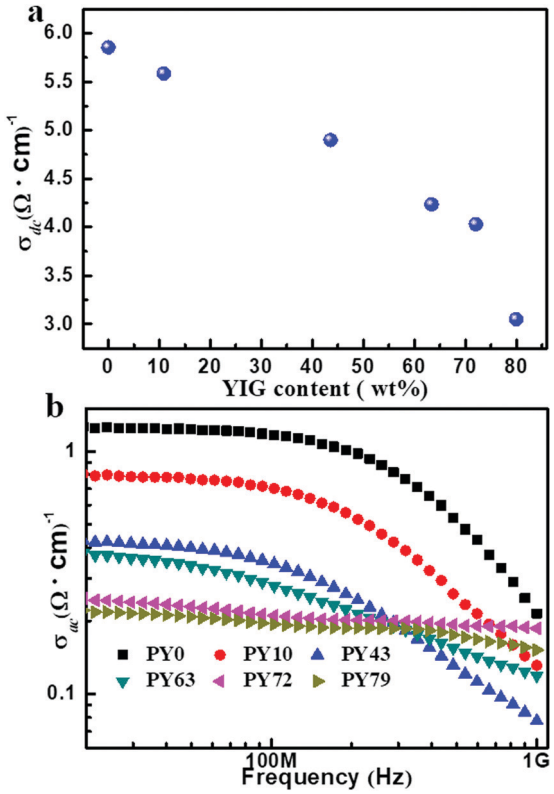

Fig. 4 DC conductivity (a) and frequency dispersions of AC conductivity (b) for PPy and its composites with different YIG contents.

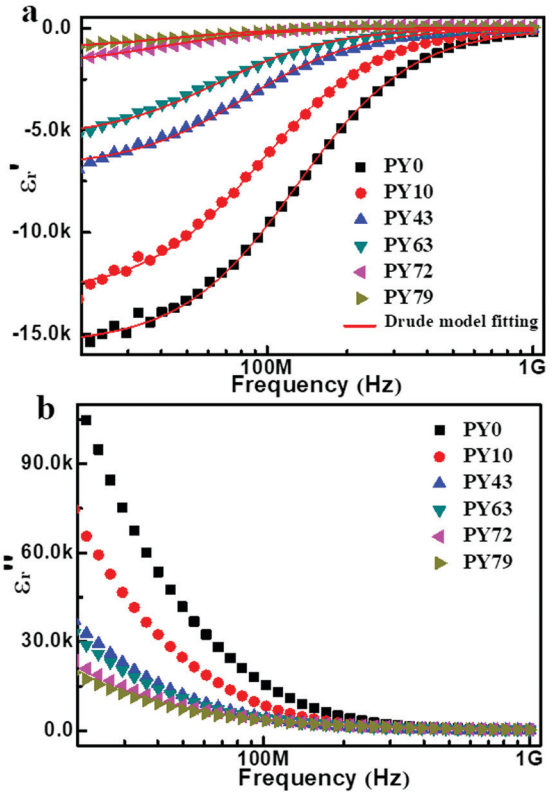

Fig. 5 Frequency dependencies of real part (a) and imaginary part (b) of permittivity for PPy and its composites with different YIG contents.

frequency of unbound electrons, at which ε_r' changes from negative to positive, and negative ε_r' appears at frequencies below ω_p. According to the Drude model, ω_p mainly depends on free carrier concentration and mass of materials, which can be represented as[65]

$$\omega_p = \sqrt{\frac{n_{eff} e^2}{m_{eff} \varepsilon_0}} \quad (3)$$

where n_{eff} is the effective density of free carriers, m_{eff} is the effective mass of the carriers, e is the electron charge (1.6×10^{-19} C), and ε_0 is the permittivity of free space (8.85×10^{-12} F m^{-1}); ω_τ is the collision frequency of free carriers and can be expressed as follows:[66]

$$\omega_\tau = \frac{n_{eff} e^2}{m_{eff} \sigma_{dc}} \quad (4)$$

In our obtained composites, the increase in YIG loading led to reduced n_{eff} owing to the formation of less PPy networks, while m_{eff} became larger due to the enhanced constraint of YIG particles on the movement of free carriers.[20,67] Hence, according

Table 1 Fitting coefficients (R^2) and parameters (ω_p and ω_τ) for PPy and its composites

Sample	PY0	PY10	PY43	PY63	PY72	PY79
ω_p/GHz	101	68.3	42.9	30	10.5	8.4
ω_τ/GHz	0.81	0.60	0.52	0.41	0.25	0.26
R^2	0.9986	0.9988	0.9980	0.9968	0.9595	0.9649

to eqn (3) and (4), ω_p and ω_τ decrease as the YIG loading increases. Meanwhile, the absolute value of ε_r' also decreased on increasing the YIG content, which was attributed to the lowered n_{eff} and increased m_{eff}. Considering all the above-mentioned discussion, it is reasonable to believe that tunable negative ε_r' (*i.e.*, the magnitude and frequency band) is achieved by controlling the content and distribution of YIG particles. Due to the observed tunable negative ε_r', our composites can be excellently applied in a capacitor and wave filter and in electromagnetic shielding.[42,43,46,47] The ε_r''–f curves of PPy and its composites are given in Fig. 5b. The imaginary part of permittivity (ε_r'') is related to dielectric loss, which generally originates from the process of conduction and polarization.[68–70] In our obtained materials, the conduction loss can make a great contribution to ε_r'' because of their high conductivity.[71] The increasing YIG content resulted in decrease in the conduction loss; thus, ε_r'' decreased.

3.4 Magnetic performance

The complex permeability ($\mu_r^* = \mu_r' - j\mu_r''$) spectra of PPy and its composites with different YIG loadings are displayed in Fig. 6. The real part of permeability μ_r' for the composites decreases monotonously with the increasing frequency, showing a typical relaxation-type frequency dispersion (Fig. 6a);[72] moreover, clear magnetic loss peaks for the composites with high YIG loadings (>43.56 wt%) are observed (Fig. 6b). The increasing YIG loading level resulted in increase in μ_r' and μ_r''. Generally, the permeability of polycrystalline magnetic materials is related to two types of magnetizing processes, namely, domain wall and gyromagnetic spin motion and can be described as follows:[52,72,73]

$$\mu_{initial} = 1 + \chi_d + \chi_s \quad (5)$$

Here, χ_d and χ_s are the magnetic susceptibilities of the domain-wall and gyromagnetic spin motions, respectively; μ_r' and μ_r'' can also be expressed as follows:[52,74,75]

$$\mu_r' = 1 + \frac{\chi_{d0}\omega_d^2(\omega_d^2 - \omega^2)}{(\omega_d^2 - \omega^2)^2 + \omega^2\beta^2} + \frac{\chi_{s0}\omega_s^2[(\omega_s^2 - \omega^2) + \omega^2\alpha^2]}{[\omega_s^2 - \omega^2(1+\alpha^2)]^2 + 4\omega^2\omega_s^2\alpha^2} \quad (6)$$

$$\mu_r'' = \frac{\chi_{d0}\omega\beta\omega_d^2}{(\omega_d^2 - \omega^2)^2 + \omega^2\beta^2} + \frac{\chi_{s0}\omega_s\omega\alpha[\omega_s^2 + \omega^2(1+\alpha^2)]}{[\omega_s^2 - \omega^2(1+\alpha^2)]^2 + 4\omega^2\omega_s^2\alpha^2} \quad (7)$$

Here, ω_d (ω_s), χ_{d0} (χ_{s0}) and α (β) are the resonance angular frequency, static magnetic susceptibility and damping factor for the domain-wall (gyromagnetic spin) component, respectively. The complex permeability spectra of PY79 sample were fitted using the formulas. It was found that the fitting curves (solid lines) coincided well with the experimental data (dotted lines), and the fitting coefficients R^2 are more than 0.97. The calculated ω_d and ω_s values

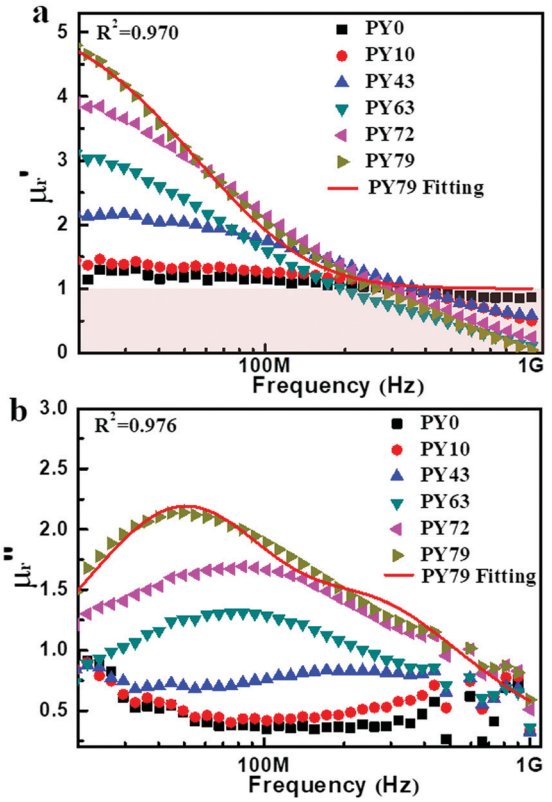

Fig. 6 Frequency dependencies of real part (a) and imaginary part (b) of permeability for PPy and its composites with different YIG contents.

are ~535 MHz and ~4.6 GHz, respectively. This indicates that the domain-wall resonance plays an important role for the permeability frequency dispersion in our test frequency band, while the gyromagnetic spin resonance occurs at higher frequency ranges.[66] It is worth mentioning that the μ_r' values of all the samples were less than 1 at the high-frequency regime, exhibiting diamagnetic responses.[76] During the magnetism measurements, many current loops were induced in the formed conducting networks under a high-frequency electromagnetic field, thus generating other electromagnetic fields to resist the external electromagnetic field.[20] Hence, the diamagnetic property ($\mu_r' < 1$) was observed at high frequencies. Furthermore, negative μ_r' has been reported in YIG and its composites in the microwave range and can be tuned by applying external DC magnetic fields.[25,52,77] It seems reasonable to believe that negative permeability can be achieved in our obtained composites at higher frequencies (>1 GHz) or by applying a DC magnetic field. The related work will be carried out in the future.

4. Conclusion

PPy composites with different YIG particle loadings were obtained through a surface-initiated polymerization method. The composites showed a metal-like conduction behavior due to the formation of PPy conducting networks, and higher YIG loadings led to decrease in conductivity. A negative permittivity behavior was also observed in the PPy composites, which was ascribed to the low-frequency plasmonic state of unbound

electrons in the PPy networks. The Drude model was used to describe the frequency dispersion of negative permittivity. With the increase in YIG loading, the plasma frequency shifted to lower frequencies, and the magnitude (absolute value) of negative permittivity also became smaller. In addition, a relaxation-type frequency dispersion of magnetic permeability was obtained in the composites, which resulted from the combination of magnetic resonance of YIG particles and diamagnetic response of PPy networks. Our work provides new opportunities for the development of random polymer metamaterials. Meanwhile, these unique composites with the conducive polymer and magnetic or other functional particles[78] can be used for many other applications such as in giant magnetoresistance sensors,[78a] strain sensors,[79] electromagnetic interface (EMI) shielding,[80] environmental remediation,[81] and structural composites.[82]

Conflicts of interest

There are no conflicts to declare.

Acknowledgements

This work was financially supported by the National Basic Research Program of China (973 Program, No. 2014CB643306), National Natural Science Foundation of China (No. 51601105, 51402170, 51602194 and 51602195), and the Natural Science Foundation of Shandong Province (No. ZR2016EMM09). C. Cheng acknowledges the support from the program for outstanding PhD candidate of Shandong University.

References

1 (*a*) N. I. Zheludev, *Science*, 2010, **328**, 582–583; (*b*) N. I. Zheludev and Y. S. Kivshar, *Nat. Mater.*, 2012, **11**, 917.
2 (*a*) C. Cheng, R. Fan, Z. Wang, Q. Shao, X. Guo, P. Xie, Y. Yin, Y. Zhang, L. An, Y. Lei, J. Ryu, A. Shankar and Z. Guo, *Carbon*, 2017, **125**, 103–112; (*b*) K. Sun, P. Xie, Z. Wang, T. Su, Q. Shao, J. Ryu, X. Zhang, J. Guo, A. Shankar, J. Li, R. Fan, D. Cao and Z. Guo, *Polymer*, 2017, **125**, 50–57.
3 D. R. Smith, J. B. Pendry and M. C. Wiltshire, *Science*, 2004, **305**, 788–792.
4 W. Fan, B. Yan, Z. Wang and L. Wu, *Sci. Adv.*, 2016, **2**, e1600901.
5 S. H. Lee, C. M. Park, Y. M. Seo and C. K. Kim, *Phys. Rev. B: Condens. Matter Mater. Phys.*, 2010, **81**, 241102.
6 J. Chen, Y. Wang, B. Jia, T. Geng, X. Li, L. Feng, W. Qian, B. Liang, X. Zhang and M. Gu, *Nat. Photonics*, 2011, **5**, 239.
7 B. Luk'yanchuk, N. I. Zheludev, S. A. Maier, N. J. Halas, P. Nordlander, H. Giessen and C. T. Chong, *Nat. Mater.*, 2010, **9**, 707.
8 P. Tassin, T. Koschny, M. Kafesaki and C. M. Soukoulis, *Nat. Photonics*, 2012, **6**, 259.
9 C. M. Watts, X. Liu and W. J. Padilla, *Adv. Mater.*, 2012, **24**, OP98–OP120.
10 L. Lv, J. Liu, H. Liu, C. Liu, Y. Lu, K. Sun, R. Fan, N. Wang, N. Lu and Z. Guo, *Eng. Sci.*, 2018, **2**, 26–42.
11 Y. Liu and X. Zhang, *Chem. Soc. Rev.*, 2011, **40**, 2494–2507.
12 H. Chen, *J. Mater. Chem.*, 2011, **21**, 6452–6463.
13 H. Wu, X. Huang and L. Qian, *Eng. Sci.*, 2018, **2**, 17–25, DOI: 10.30919/es8d656.
14 (*a*) J. M. Manimala, P. P. Kulkarni and K. Madhamshetty, *Adv. Compos. Hybrid. Mater.*, 2018, 1–12; (*b*) H. Gu, H. Zhang, C. Gao, C. Liang, J. Gu and Z. Guo, *ES Mater. Manuf.*, 2018, **1**, 3–12, DOI: 10.30919/esmm5f108.
15 D. R. Smith, W. J. Padilla, D. Vier, S. C. Nemat-Nasser and S. Schultz, *Phys. Rev. Lett.*, 2000, **84**, 4184.
16 B. Li, G. Sui and W. H. Zhong, *Adv. Mater.*, 2009, **21**, 4176–4180.
17 X. Yao, X. Kou, J. Qiu and M. Moloney, *J. Phys. Chem. C*, 2016, **120**, 4937–4944.
18 Z. Shi, S. Chen, K. Sun, X. Wang, R. Fan and X. Wang, *Appl. Phys. Lett.*, 2014, **104**, 252908.
19 X. Wang, Z. Shi, M. Chen, R. Fan, K. Yan, K. Sun, S. Pan and M. Yu, *J. Am. Ceram. Soc.*, 2014, **97**, 3223–3229.
20 Z. C. Shi, R. H. Fan, K. L. Yan, K. Sun, M. Zhang, C. G. Wang, X. F. Liu and X. H. Zhang, *Adv. Funct. Mater.*, 2013, **23**, 4123–4132.
21 Z. Shi, R. Fan, Z. Zhang, L. Qian, M. Gao, M. Zhang, L. Zheng, X. Zhang and L. Yin, *Adv. Mater.*, 2012, **24**, 2349–2352.
22 Z. Shi, R. Fan, Z. Zhang, H. Gong, J. Ouyang, Y. Bai, X. Zhang and L. Yin, *Appl. Phys. Lett.*, 2011, **99**, 032903.
23 T. Tsutaoka, T. Kasagi, S. Yamamoto and K. Hatakeyama, *J. Magn. Magn. Mater.*, 2015, **383**, 139–143.
24 T. Tsutaoka, T. Kasagi, S. Yamamoto and K. Hatakeyama, *Appl. Phys. Lett.*, 2013, **102**, 181904.
25 T. Tsutaoka, K. Fukuyama, H. Kinoshita, T. Kasagi, S. Yamamoto and K. Hatakeyama, *Appl. Phys. Lett.*, 2013, **103**, 261906.
26 T. Tsutaoka, H. Massango, T. Kasagi, S. Yamamoto and K. Hatakeyama, *Appl. Phys. Lett.*, 2016, **108**, 191904.
27 M. Chen, M. Gao, F. Dang, N. Wang, B. Zhang and S. Pan, *Ceram. Int.*, 2016, **42**, 6444–6449.
28 B. Qiu, J. Guo, Y. Wang, X. Wei, Q. Wang, D. Sun, M. A. Khan, D. P. Young, R. O'Connor and X. Huang, *J. Mater. Chem. C*, 2015, **3**, 3989–3998.
29 H. Gu, J. Guo, Q. He, Y. Jiang, Y. Huang, N. Haldolaarachige, Z. Luo, D. P. Young, S. Wei and Z. Guo, *Nanoscale*, 2014, **6**, 181–189.
30 J. Zhu, H. Gu, Z. Luo, N. Haldolaarachige, D. P. Young, S. Wei and Z. Guo, *Langmuir*, 2012, **28**, 10246–10255.
31 R. Kohlman, J. Joo, Y. Wang, J. Pouget, H. Kaneko, T. Ishiguro and A. Epstein, *Phys. Rev. Lett.*, 1995, **74**, 773.
32 V. Prigodin and A. Epstein, *Synth. Met.*, 2001, **125**, 43–53.
33 J. Zhu, S. Wei, L. Zhang, Y. Mao, J. Ryu, P. Mavinakuli, A. B. Karki, D. P. Young and Z. Guo, *J. Phys. Chem. C*, 2010, **114**, 16335–16342.
34 J. Guo, H. Gu, H. Wei, Q. Zhang, N. Haldolaarachchige, Y. Li, D. P. Young, S. Wei and Z. Guo, *J. Phys. Chem. C*, 2013, **117**, 10191–10202.
35 X. Zhang, S. Wei, N. Haldolaarachchige, H. A. Colorado, Z. Luo, D. P. Young and Z. Guo, *J. Phys. Chem. C*, 2012, **116**, 15731–15740.

36 H. Gu, J. Guo, M. A. Khan, D. P. Young, T. Shen, S. Wei and Z. Guo, *Phys. Chem. Chem. Phys.*, 2016, **18**, 19536–19543.
37 H. Gu, Y. Huang, X. Zhang, Q. Wang, J. Zhu, L. Shao, N. Haldolaarachchige, D. P. Young, S. Wei and Z. Guo, *Polymer*, 2012, **53**, 801–809.
38 X. Kou, X. Yao and J. Qiu, *Org. Electron.*, 2016, **38**, 42–47.
39 J. Zhu, X. Zhang, N. Haldolaarachchige, Q. Wang, Z. Luo, J. Ryu, D. P. Young, S. Wei and Z. Guo, *J. Mater. Chem.*, 2012, **22**, 4996–5005.
40 X. Kou, X. Yao and J. Qiu, *J. Polym. Sci., Part B: Polym. Phys.*, 2017, **55**, 1724–1729.
41 X. Yao, X. Kou and J. Qiu, *Carbon*, 2016, **107**, 261–267.
42 C. Cheng, R. Fan, L. Qian, X. Wang, L. Dong and Y. Yin, *RSC Adv.*, 2016, **6**, 87153–87158.
43 M. Zhong, *Opt. Mater.*, 2015, **47**, 62–66.
44 N. Engheta, *Science*, 2007, **317**, 1698–1702.
45 Q. Yuchang, W. Qinlong, L. Fa and Z. Wancheng, *J. Mater. Chem. C*, 2016, **4**, 4853–4862.
46 R. Gholipur, Z. Khorshidi and A. Bahari, *ACS Appl. Mater. Interfaces*, 2017, **9**, 12528–12539.
47 J. Wang, Z. Shi, F. Mao, S. Chen and X. Wang, *ACS Appl. Mater. Interfaces*, 2017, **9**, 1793–1800.
48 (*a*) Z. Shi, J. Wang, F. Mao, C. Yang, C. Zhang and R. Fan, *J. Mater. Chem. A*, 2017, **5**, 14575–14582; (*b*) J. Wang, Z. Shi, X. Wang, X. Mai, R. Fan, H. Liu, X. Wang and Z. Guo, *Eng. Sci.*, 2018, **4**, 79–86, DOI: 10.30919/es8d759.
49 K. Bi, W. Zhu, M. Lei and J. Zhou, *Appl. Phys. Lett.*, 2015, **106**, 173507.
50 A. Sposito, G. B. Stenning, S. A. Gregory, P. A. de Groot and R. W. Eason, *Thin Solid Films*, 2014, **568**, 31–37.
51 D. T. T. Nguyet, N. P. Duong, T. Satoh, L. N. Anh and T. D. Hien, *J. Alloys Compd.*, 2012, **541**, 18–22.
52 T. Tsutaoka, T. Kasagi and K. Hatakeyama, *J. Appl. Phys.*, 2011, **110**, 053909.
53 K. Sun, R. Fan, Y. Yin, J. Guo, X. F. Li, Y. Lei, L. An, C. Cheng and Z. Guo, *J. Phys. Chem. C*, 2017, **121**, 7564–7571.
54 K. Sun, Z. Zhang, L. Qian, F. Dang, X. Zhang and R. Fan, *Appl. Phys. Lett.*, 2016, **108**, 061903.
55 M. Chen, X. Wang, Z. Zhang, K. Sun, C. Cheng and F. Dang, *Mater. Des.*, 2016, **97**, 454–458.
56 P. Mavinakuli, S. Wei, Q. Wang, A. B. Karki, S. Dhage, Z. Wang, D. P. Young and Z. Guo, *J. Phys. Chem. C*, 2010, **114**, 3874–3882.
57 P. M. Carrasco, H. J. Grande, M. Cortazar, J. M. Alberdi, J. Areizaga and J. A. Pomposo, *Synth. Met.*, 2006, **156**, 420–425.
58 C. Xu, J. Sun and L. Gao, *J. Mater. Chem.*, 2011, **21**, 11253–11258.
59 X. Yao, X. Kou and J. Qiu, *Mater. Chem. Phys.*, 2018, **208**, 177–182.
60 C. Hou, Y. Hou, Y. Fan, Y. Zhai, Y. Wang, Z. Sun, R. Fan, F. Dang and J. Wang, *J. Mater. Chem. A*, 2018, **6**, 6967–6976.
61 C. Hou, Z. Tai, L. Zhao, Y. Zhai, Y. Hou, Y. Fan, F. Dang, J. Wang and H. Liu, *J. Mater. Chem. A*, 2018, **6**, 9723–9736.
62 B. Zhao, J. Deng, R. Zhang, L. Liang, B. Fan, Z. Bai, G. Shao and C. Park, *Eng. Sci.*, 2018, **3**, 5–40.
63 C. Cheng, R. Fan, Y. Ren, T. Ding, L. Qian, J. Guo, X. Li, L. An, Y. Lei and Y. Yin, *Nanoscale*, 2017, **9**, 5779–5787.
64 (*a*) S. Linden, C. Enkrich, M. Wegener, J. Zhou, T. Koschny and C. M. Soukoulis, *Science*, 2004, **306**, 1351–1353; (*b*) P. Xie, Z. Wang, Z. Zhang, R. Fan, C. Cheng, H. Liu, Y. Liu, T. Li, C. Yan, N. Wang and Z. Guo, *J. Mater. Chem. C*, 2018, **6**, 5239–5249.
65 R. Friend, *Nature*, 2006, **441**, 37.
66 K. Sun, R. Fan, Z. Zhang, K. Yan, X. Zhang, P. Xie, M. Yu and S. Pan, *Appl. Phys. Lett.*, 2015, **106**, 172902.
67 J. B. Pendry, A. Holden, W. Stewart and I. Youngs, *Phys. Rev. Lett.*, 1996, **76**, 4773.
68 C. W. Nan, Y. Shen and J. Ma, *Annu. Rev. Mater. Res.*, 2010, **40**, 131–151.
69 (*a*) C. Wu, X. Huang, X. Wu, L. Xie, K. Yang and P. Jiang, *Nanoscale*, 2013, **5**, 3847–3855; (*b*) P. Xie, B. He, F. Dang, J. Lin, R. Fan, C. Hou, H. Liu, J. Zhang, Y. Ma and Z. Guo, *J. Mater. Chem. C*, 2018, **6**, 8812–8822; (*c*) J. Guo, H. Song, H. Liu, C. Luo, Y. Ren, T. Ding, M. A. Khan, D. P. Young, X. Liu, X. Zhang, J. Kong and Z. Guo, *J. Mater. Chem. C*, 2017, **5**, 5334–5344.
70 X. Fan and X. Yin, *Adv. Compos. Hybrid Mater.*, 2018, 1–11.
71 H. Luo and J. Qiu, *Ceram. Int.*, 2019, **45**, 843–848.
72 T. Tsutaoka, *J. Appl. Phys.*, 2003, **93**, 2789–2796.
73 N. Wu, J. Qiao, J. Liu, W. Du, D. Xu and W. Liu, *Adv. Compos. Hybrid Mater.*, 2018, **1**, 149–159.
74 K. Yan, R. Fan, Z. Shi, M. Chen, L. Qian, Y. Wei, K. Sun and J. Li, *J. Mater. Chem. C*, 2014, **2**, 1028–1033.
75 H. Wu, Y. Zhang, R. Yin, W. Zhao, X. Li and L. Qian, *Adv. Compos. Hybrid Mater.*, 2018, **1**, 168–176.
76 X. Hu, C. T. Chan, J. Zi, M. Li and K.-M. Ho, *Phys. Rev. Lett.*, 2006, **96**, 223901.
77 Z. Shi, R. Fan, Z. Zhang, K. Yan, X. Zhang, K. Sun, X. Liu and C. Wang, *J. Mater. Chem. C*, 2013, **1**, 1633–1637.
78 (*a*) H. Gu, H. Zhang and J. Lin, *et al.*, *Polymer*, 2018, **143**, 324–330; (*b*) Z. Zhao, P. Bai and L. Li, *et al.*, *Materials*, 2019, **12**, 330; (*c*) Y. Zhao, B. Zhang, H. Hou, W. Chen and M. Wang, *J. Mater. Sci. Technol.*, 2019, DOI: 10.1016/j.jmst.2018.12.009; (*d*) Y. Zhao, S. Deng and H. Liu, *et al.*, *Comput. Mater. Sci.*, 2018, **154**, 365–370; (*e*) Y. Sheng, J. Yang and F. Wang, *et al.*, *Appl. Surf. Sci.*, 2019, **465**, 154–163; (*f*) Y. Zhao, X. Tian and B. Zhao, *et al.*, *Sci. Adv. Mater.*, 2018, **10**, 1793–1804; (*g*) Y. Zhao, L. Qi, Y. Jin, K. Wang, J. Tian and P. Han, *J. Alloys Compd.*, 2015, **647**, 1104–1110; (*h*) J. Tian, Q. Shao and J. Zhao, *et al.*, *J. Colloid Interface Sci.*, 2019, **541**, 18–29; (*i*) D. Pan, S. Ge and J. Zhao, *et al.*, *Ind. Eng. Chem. Res.*, 2019, **58**, 836–848; (*j*) W. Xie, X. Zhu, S. Yi, J. Kuang, H. Cheng, W. Tang and Y. Deng, *Mater. Des.*, 2016, **90**, 38–46.
79 (*a*) H. Liu, Q. Li, S. Zhang, R. Yin, X. Liu, Y. He, K. Dai, C. Shan, J. Guo, C. Liu, C. Shen, X. Wang, N. Wang, Z. Wang, R. Wei and Z. Guo, *J. Mater. Chem. C*, 2018, **6**, 12121–12141; (*b*) H. Gu, H. Zhang and C. Ma, *et al.*, *J. Mater. Chem. C*, 2019, **7**, 2353–2360; (*c*) H. Wei, H. Wang and Y. Xia, *et al.*, *J. Mater. Chem. C*, 2018, **6**, 12446–12467; (*d*) Y. Lu, M. C. Biswas, Z. Guo, J. Jeon and E. K. Wujcik, *Biosens. Bioelectron.*, 2019, **123**, 167–177.

80 (*a*) N. Wu, C. Liu and D. Xu, *et al.*, *J. Mater. Chem. C*, 2019, **7**, 1659–1669; (*b*) W. Xie, X. Zhu, S. Yi, J. Kuang, H. Cheng, W. Tang and Y. Deng, *Mater. Des.*, 2016, **90**, 38–46; (*c*) C. Wang, Z. He and X. Xie, *et al.*, *Macromol. Mater. Eng.*, 2018, **3**, 1700462; (*d*) C. Wang, V. Murugadoss and J. Kong, *et al.*, *Carbon*, 2018, **140**, 696–733; (*e*) D. Jiang, V. Murugadoss and Y. Wang, *et al.*, *Polym. Rev.*, 2018, DOI: 10.1080/15583724.2018.1546737; (*f*) Z. Wang, R. Wei and J. Gu, *et al.*, *Carbon*, 2018, **139**, 1126–1135; (*g*) L. Wang, H. Qiu and C. Liang, *et al.*, *Carbon*, 2019, **141**, 506–514; (*h*) N. Wu, D. Xu and Z. Wang, *et al.*, *Carbon*, 2019, **145**, 433–444; (*i*) N. Wu, C. Liu, D. Xu, J. Liu, W. Liu, Q. Shao and Z. Guo, *ACS Sustainable Chem. Eng.*, 2018, **6**, 12471–12480.

81 (*a*) Y. Qian, Y. Yuan and H. Wang, *et al.*, *J. Mater. Chem. A*, 2018, **6**, 24676–24685; (*b*) K. Gong, Q. Hu, Y. Xiao and X. Cheng, *et al.*, *J. Mater. Chem. A*, 2018, **6**, 11119–11128; (*c*) K. Gong, S. Guo and Y. Zhao, *et al.*, *J. Mater. Chem. A*, 2018, **6**, 16824–16832; (*d*) H. Zhang, S. Lyu and X. Zhou, *et al.*, *J. Colloid Interface Sci.*, 2019, **536**, 245–251; (*e*) Z. Li, B. Wang and X. Qin, *et al.*, *ACS Sustainable Chem. Eng.*, 2018, **6**, 13747–13755; (*f*) K. Gong, Q. Hu, L. Yao, M. Li, D. Sun, Q. Shao, B. Qiu and Z. Guo, *ACS Sustainable Chem. Eng.*, 2018, **6**, 7283–7291; (*g*) Y. Wang, P. Zhou, S. Luo, X. Liao, B. Wang, Q. Shao, X. Guo and Z. Guo, *Langmuir*, 2018, **34**, 7859–7868; (*h*) Y. Ma, L. Lyu and Y. Guo, *et al.*, *Polymer*, 2017, **128**, 12–23; (*i*) Y. Wang, P. Zhou and S. Luo, *et al.*, *Adv. Polym. Technol.*, 2018, **37**, 2981–2996; (*j*) Z. Zhao, H. An and J. Lin, *et al.*, *Chem. Rec.*, 2019, DOI: 10.1002/tcr.201800153.

82 (*a*) Z. Wu, H. Cui and L. Chen, *et al.*, *Compos. Sci. Technol.*, 2018, **164**, 195–203; (*b*) H. Gu, H. Zhang and C. Ma, *et al.*, *Carbon*, 2019, **142**, 131–140; (*c*) J. Zhang, P. Li and Z. Zhang, *et al.*, *J. Colloid Interface Sci.*, 2019, **542**, 159–167; (*d*) Y. Li, T. Jing and G. Xu, *et al.*, *Polymer*, 2018, **149**, 13–22; (*e*) M. Dong, Q. Li and H. Liu, *et al.*, *Polymer*, 2018, **158**, 381–390; (*f*) Z. Wu, S. Gao, L. Chen and D. Jiang, *et al.*, *Macromol. Chem. Phys.*, 2017, **218**, 1700357; (*g*) J. Zhang, H. Li and B. Zhou, *et al.*, *J. Mater. Chem. C*, 2018, **6**, 8360–8371; (*h*) Y. He, S. Yang and H. Liu, *et al.*, *J. Colloid Interface Sci.*, 2018, **517**, 40–51; (*i*) X. Liu, Y. Pan and G. Zheng, *et al.*, *Macromol. Mater. Eng.*, 2018, **303**(8), 1800035; (*j*) K. Sun, R. Fan and X. Zhang, *et al.*, *J. Mater. Chem. C*, 2018, **6**, 2925–2943.